remote sensing

Article

A Data Quality Assessment Approach for High-Precision GNSS Continuously Operating Reference Stations (CORS) with Case Studies in Hong Kong and Canada/USA

Lawrence Lau * and Kai-Wing Tai

Department of Land Surveying and Geo-Informatics, The Hong Kong Polytechnic University, Hong Kong SAR, China
* Correspondence: lsgi-lawrence.lau@polyu.edu.hk; Tel.: +852-27665964

Abstract: Centimeter-level or better positioning accuracy is needed in engineering surveying applications. When employing the Global Navigation Satellite System (GNSS) in engineering surveying, the high-precision real-time kinematic (RTK) positioning method must be used to achieve such positioning accuracy. Currently, precise point positioning (PPP) cannot reliably achieve the positioning accuracy needed for engineering surveying in real time. The high-precision RTK positioning method needs carrier-phase measurements and a reference station/network. Surveyors may not need a GNSS receiver in their organizations/companies to act as the reference station. Continuously Operating Reference Stations (CORS), run by international/national organizations/agencies or private companies such as GNSS receiver manufacturers, let users freely access the raw GNSS measurements or corrections for real-time and post-processing applications. The positioning accuracy of the GNSS rover is affected by the data quality of the reference stations, including virtual reference stations (VRS). The International GNSS Service (IGS) currently provides the number of cycle slips and the L1 and L2 average pseudorange multipath errors per station daily. The US National Geodetic Survey (NGS) provides daily station coordinate residuals. Carrier-phase data quality of the CORS stations is not provided by their organizations/agencies. Nowadays, many CORS stations track multi-GNSS satellites. This paper proposes a multi-GNSS and multi-frequency data quality assessment approach for CORS stations with a focus on carrier-phase data quality. The proposed approach is demonstrated with case studies on IGS/CORS networks in Hong Kong and Canada/USA. In other words, a strategy to obtain non-linear combined carrier-phase multipath errors and noise is proposed in this work. The data quality of a CORS station depends on the site environment, monument type and height, and GNSS receiver/antenna. An account of the data quality at some selected stations is given; the main focus of the paper is on the proposed data quality assessment approach.

Keywords: Continuously Operating Reference Stations (CORS); GNSS data quality; multipath errors; random errors; Hong Kong Satellite Positioning Reference Station Network (SatRef); IGS network

Citation: Lau, L.; Tai, K.-W. A Data Quality Assessment Approach for High-Precision GNSS Continuously Operating Reference Stations (CORS) with Case Studies in Hong Kong and Canada/USA. *Remote Sens.* **2023**, *15*, 1925. https://doi.org/10.3390/rs15071925

Academic Editors: Jong-Hoon Won and Nobuaki Kubo

Received: 21 February 2023
Revised: 29 March 2023
Accepted: 30 March 2023
Published: 3 April 2023

1. Introduction

The Global Positioning System (GPS) was developed for single-point positioning (i.e., Standard/Precise Positioning Service). The use of carrier-phase measurements in relative positioning was explored by [1–3]. Since then, GPS has been widely used in high-precision positioning applications, such as attitude determination [4,5], geodetic surveying [6,7], geodynamic and geophysical studies [8,9], and engineering surveying [10]. A reference receiver is needed for relative positioning, and the determined position of the rover station is aligned in the same reference frame as the reference station. Organizations/companies needed a GPS receiver for the reference station and a GPS receiver for the rover station in the 1980s and 1990s. The US National Geodetic Survey (NGS) and the International GNSS Service (IGS; was called the International GPS Service for Geodynamics) developed the

Continuously Operating Reference Stations (CORS; also known as tracking stations) for precise orbit determination in the 1990s. Moreover, the CORS stations serve as the reference stations for relative positioning. In addition, some GPS receiver manufacturers have built CORS in some countries/regions, such as Leica and Trimble. Surveyors only need a rover receiver for engineering surveying when there is a CORS network in the region.

Usually, the nearest CORS station is selected for baseline processing. In baseline processing, any errors at the reference station are propagated to the estimated position of the rover. In network real-time kinematic (RTK) approaches, such as the Master-Auxiliary Concept (MAC) [11] and Virtual Reference Station (VRS) [12], errors at reference stations affect the RTK corrections, modeled biases/errors, and raw measurements. Site selection is a step in network RTK approaches. We prefer selecting reference stations with high-quality raw measurements over selecting the nearest reference stations. The quality of raw measurements at reference stations is affected by cycle slips, measurement noise, and multipath errors. The IGS website does provide hourly time-series plots of the number of cycle slips in GPS L1 and L2 measurements and pseudorange multipath errors in GPS L1 and L2 measurements (i.e., MP1 and MP2) per station. It is worth mentioning that "multipath mitigation should be disabled in the GNSS receiver" [13] (guideline no. 2.2.19), excluding special antenna designs such as choke-ring antennas.

GPS and GLONASS modernization is being undertaken. Galileo will have its full operational capacity (FOC) soon (scheduled for 2020; it has 23 "usable" satellites as of 20 June 2022). The BeiDou Navigation Satellite System (BDS) started FOC in June 2020. The Global Navigation Satellite System (GNSS) is the collective term for GPS, GLONASS, Galileo, and BDS. Currently, IGS only provides the daily average pseudorange multipath errors in GPS L1 and L2 measurements (i.e., average MP1 and MP2) and the number of cycle slips (but not specific to L1 or L2) per CORS/tracking station. High-precision GNSS users may want to use either GPS, GLONASS, Galileo, or BDS only. The quality of GNSS measurements (i.e., all constellations and multi-frequency) at each CORS station is essential for station selection in baseline post-processing and (conventional/network) RTK.

This paper proposes a multi-GNSS and multi-frequency data quality assessment approach for CORS stations with a focus on carrier-phase data quality. There is no absolute approach for GNSS data quality assessment. The proposed approach is designed to minimize the effect of other GNSS biases/errors on the assessed data quality. The proposed approach is demonstrated with case studies on the Hong Kong and Canada/USA CORS networks. An analysis of the data quality at some selected CORS stations will be given. GNSS CORS data quality is affected by the antenna and receiver hardware and firmware, the monument type and height, the site environment and location, etc. CORS organizations/agencies may implement the proposed approach to assess the data quality of their CORS stations, and they may try to find out the reasons for the stations with poor data quality assessment results and then propose a data quality improvement plan for the stations. This work is significant because small carrier-phase noise and multipath errors at CORS stations may affect the ambiguity resolution and lead to wrong/inaccurate rover position solutions [14,15].

2. Materials and Methods

2.1. Literature Review and Significance of Research

2.1.1. GNSS Biases and Errors

GNSS biases can be classified as dispersive or non-dispersive. The ionospheric effect is a dispersive bias, and the tropospheric effect is a non-dispersive bias. Both ionospheric and tropospheric effects decorrelate to the increase in baseline length. GNSS errors include the satellite clock error, receiver clock errors, multipath errors, and measurement noise/random errors. Sophisticated models of the ionospheric and tropospheric effects and other GNSS biases and errors have recently been developed with the GNSS CORS network data. Multipath errors and measurement noises are site-dependent and receiver-dependent [16]. Differencing cannot eliminate multipath errors and measurement noise but can amplify the errors because of the error propagation of the satellite-receiver pairs in differencing. Multipath occurs when the direct signal from a satellite is mixed with the reflected signal in the vicinity of the rover antenna [15,17]. Site-dependent multipath errors can be mitigated by sidereal filters [18,19] and empirical multipath maps [20,21]. Both sidereal filtering and empirical multipath mapping methods need double-difference carrier-phase residuals at static baselines. In GNSS data processing, especially in kinematic positioning, multipath errors at the reference stations are usually ignored (i.e., multipath errors are not in the functional model) because CORS sites are usually considered "multipath-free". In CORS sites, geodetic-grade choke-ring antennas are installed on tall pillars/monuments, and the antennas are usually far from any reflectors in the environments. However, data at CORS stations are still contaminated in practice by near-field multipath errors. IGS uses Translation, Editing, and Quality Checking (TEQC) software [22] to estimate the pseudorange multipath errors in GPS L1 and L2. Examples of the average MP1 and MP2 of five IGS tracking stations are shown in Table 1. The authors of [23] used TEQC software to plot MP1 and MP2 in time series and analyze the possible sources of reflected signals at a site. If the site-dependent multipath errors are not modeled in data processing, we ought to select a CORS station with low multipath errors and measurement noise as the reference station in post-processing/real-time static/kinematic baseline processing or select CORS stations with low multipath errors and measurements for post-processing/RTK network processing. Currently, information on carrier-phase multipath errors and measurement noise is not available for CORS stations. However, high-precision positioning (i.e., baseline and RTK processing) must use carrier-phase measurements. This paper proposes a multi-GNSS and multi-frequency data quality assessment approach for CORS stations with a focus on carrier-phase data quality.

Table 1. Examples of daily average MP1 and MP2 of five IGS tracking stations.

Site ID	Average MP1 (m)	Average MP2 (m)	Receiver Type	Antenna Type
AIRA	0.56	0.62	TRIMBLE NETR9	TRM59800.00
BAMF	0.66	0.61	SEPT POLARX5	SEPCHOKE_B3E6
GOL2	0.9	0.94	ASHTECH UZ-12	AOAD/M_T
JPLM	0.23	0.23	SEPT POLARX5	AOAD/M_T
NRC1	0.41	0.44	JAVAD TRE_G3TH DELTA	AOAD/M_T

2.1.2. Review of GNSS Data Quality Assessment Methods

GNSS data quality metrics include data utilization ratios, code multipath magnitudes, cycle slip occurrence rates, and signal-to-noise ratio (SNR) analysis. The authors of [24] used TEQC and Anubis software to analyze the data utilization, cycle slip ratio, and multipath of a CORS station in Guilin and compared the performance between the two tools. IGS provides typical daily data quality assessment results with TEQC for every IGS CORS, as shown in Figure 1. However, TEQC can only assess GPS, GLONASS, and Galileo (partly) data. G-Nut/Anubis can support most navigation systems, but its availability to users is limited by only offering a free version in Linux [25]. GFZRNX provides limited quality check metrics, which cannot be used for cycle slip detection and multipath estimation [26]; the tool mainly provides RINEX file editing functions.

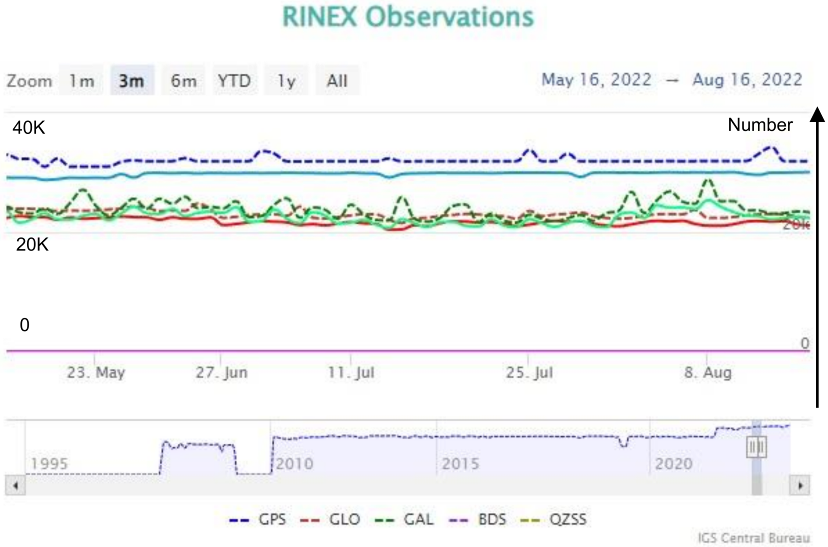

(**a**)

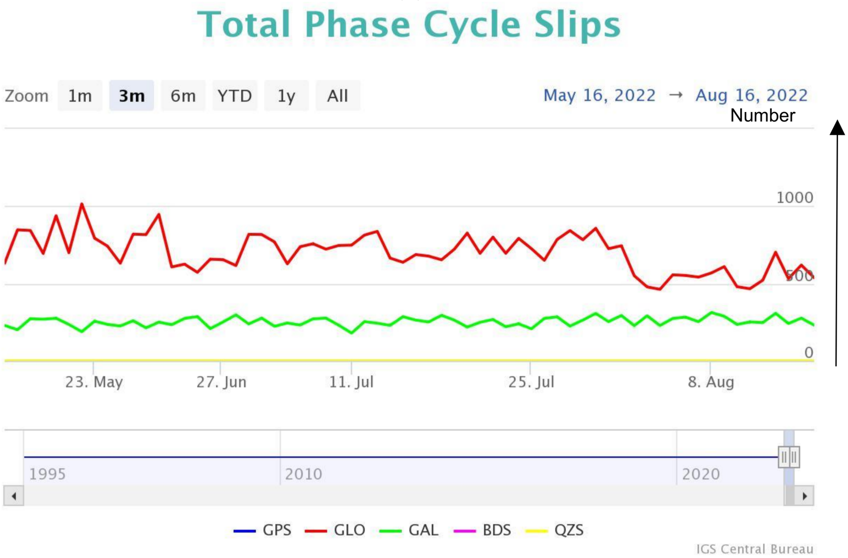

(**b**)

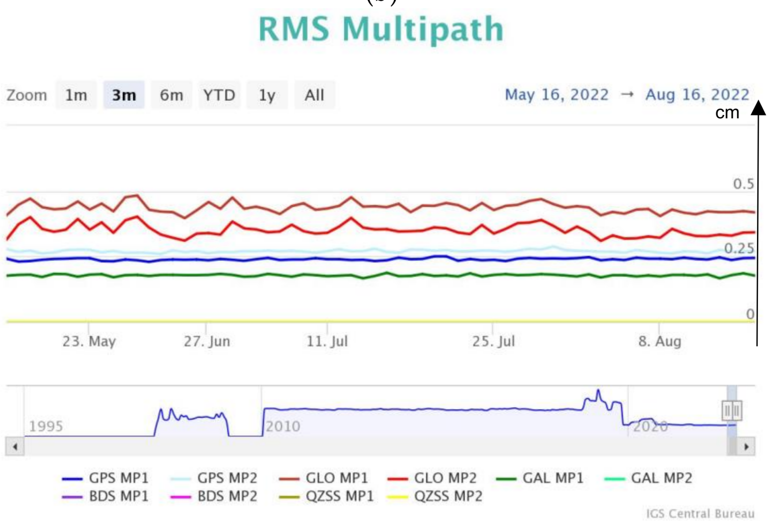

(**c**)

Figure 1. *Cont.*

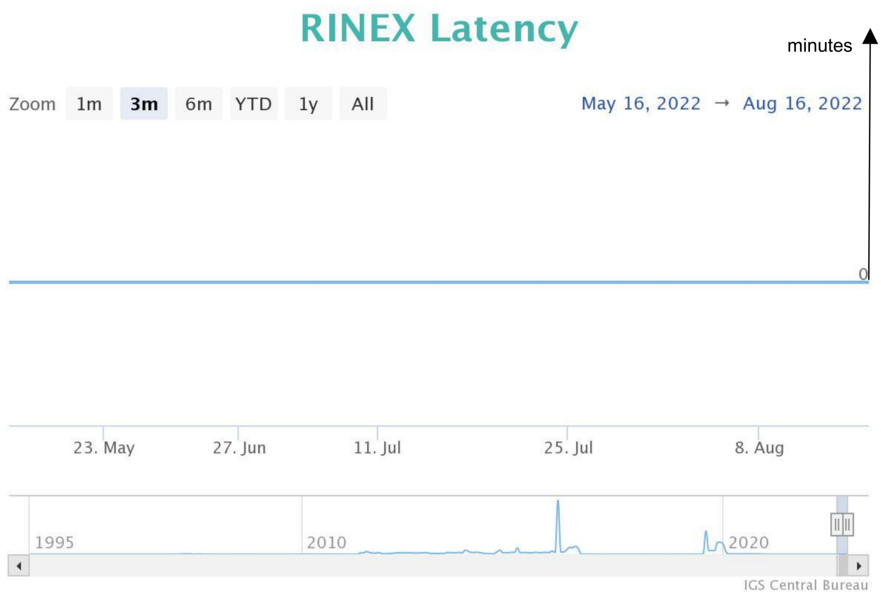

(d)

(e)

Figure 1. IGS daily data assessment results at LBCH station from 16 May to 16 August 2022. (**a**) Daily RINEX observations (no BDS and QZSS data); dotted line: expected, solid line: observed. (**b**) Cycle slips (GPS, BDS, and QZSS are always zero). (**c**) RMS multipath in meters (Galileo MP2, BDS, and QZSS are always zero). (**d**) RINEX latency in seconds (always zero). (**e**) Residuals in millimeters; green: north, purple: east, aqua: vertical. (Plots are downloaded from the IGS website; text/scale cannot be changed.)

Among all these quality-checking metrics, multipath errors and noise should be the most important because they cannot be mitigated or eliminated like other GNSS biases and errors through differencing. The multipath effect is independent for each satellite and receiver and varies with time [14,15]. With the increasing number of GNSS systems, researchers are studying the multipath effect on the multi-GNSS system. The authors of [27] (2016) investigated the measurement noise of the new GNSS signals. The authors of [28] conducted a comprehensive multipath analysis on both pseudorange and carrier-phase measurements of GPS, GLONASS, Galileo, and BeiDou. However, each observation session in the experiment was only 4 h, which did not cover the whole multipath pattern of a satellite/site. The authors of [29–31] studied the multipath effect at CORS and IGS stations and analyzed the sites and equipment with respect to the multipath effect. In this paper, a 60-day observation period was chosen to thoroughly investigate the multipath effect of GNSS satellites at the selected sites; most possible multipath errors at a site due to satellite orbiting, the sidereal day, and earth rotation are covered. In fact, one of the goals of multipath analysis is to check the data quality of GNSS stations in order to provide a better GNSS service or more information to the user. Since there are changes in satellite orbits, the site environment, and receiver/antenna hardware (including the health and stability of electronic components), data quality assessment should be carried out regularly (e.g., every year).

2.1.3. Review of Pseudorange Multipath Estimation

Pseudorange multipath is defined as the multipath errors in the pseudorange measurements (i.e., after signal processing in receiver hardware). The authors of [32] performed the pseudorange multipath estimation using triple-frequency pseudorange measurements and concluded that the triple-frequency approach can give an absolute estimate of multipath with the complete elimination of other errors. The estimation formula is:

$$\mathrm{M}_{\mathrm{P_{ijk}}} = \lambda_k^2(P_i - P_j) + \lambda_j^2(P_k - P_i) + \lambda_i^2(P_j - P_k) \tag{1}$$

where the subscripts i, j, and k denote the three frequencies of L_i, L_j, and L_k. $M_{P_{ijk}}$ denotes the ijk triple-frequency combined pseudorange multipath error, P denotes the pseudorange measurement at a frequency, and λ denotes the wavelength of a frequency. However, multipath errors and measurement noise at different frequencies are different if the signal designs (e.g., chipping rate and modulation) of frequencies are different. According to the error propagation law, the variance of the triple-frequency combined pseudorange multipath error contains the amplified measurement noise, and the noise level may be comparable to the pseudorange multipath errors. Moreover, triple-frequency tracking is still not common at CORS stations, which limits the availability of the estimation. Another weakness is that the pseudorange measurement quality of individual frequencies is not available for low-cost/single-frequency GNSS users.

In contrast to the above method, single-frequency and dual-frequency-based approaches are more commonly used. The former approach is called code-minus-carrier (CMC) [33]. *CMC* is the difference between pseudorange measurement P and carrier phase measurement (in the unit of meters) Φ:

$$CMC = P - \Phi \tag{2}$$

This method assumes the carrier-phase multipath errors are negligible when compared with the pseudorange multipath errors. Common GNSS biases and errors in pseudorange and carrier-phase measurements, such as tropospheric delay, satellite and receiver clock offsets, and satellite orbit errors, are eliminated by the differencing. However, the ionospheric effect is doubled and absorbed in the computed pseudorange multipath error (i.e., CMC). The authors of [34] used this method to test the pseudorange multipath mitigation performance of the simple-strobe and synthesized-strobe delay-locked loops (DLLs). To remedy the weakness of CMC and the insufficient observed frequencies problem, researchers usually use the linear multipath combination (i.e., *MP*) adopted in the TEQC to analyze the pseudorange multipath errors; examples are [24,30,32,35]. The MP can be computed as follows:

$$MP_i - B_i = P_i - \Phi_i - \frac{2}{\alpha - 1}(\Phi_i - \Phi_j) - 2\frac{B_j - B_i}{\alpha - 1} \tag{3}$$

where the subscripts i and j denote the frequencies of L_i and L_j, MP_i denotes the pseudorange multipath errors plus the measurement noises in L_i, P denotes the pseudorange measurement, and B denotes the carrier-phase integer ambiguity, $\alpha = \left(\frac{f_i}{f_j}\right)^2$. If we rearrange Equation (3), we obtain:

$$MP_i - P_i + \left(\frac{2}{\alpha - 1} + 1\right)\Phi_i - 2\frac{\Phi_j}{\alpha - 1} = B_i - 2\frac{B_j - B_i}{\alpha - 1} \tag{4}$$

of which, $\left(B_i - 2\frac{B_j - B_i}{\alpha - 1}\right)$ is constant for each given orbit arc (when no cycle slip), it can be subtracted by averaging it out in the final solution. Consequently, the pseudorange multipath plus noise can be written as follows:

$$MP_i = P_i - \left(\frac{2}{\alpha - 1} + 1\right)\Phi_i + 2\frac{\Phi_j}{\alpha - 1} \tag{5}$$

Equation (5) is geometry-free and ionospheric-free so it can largely reduce the error that affects the geometry-free CMC approach. Although carrier-phase multipath errors and noise exist in the equation, those values are comparatively much smaller than pseudorange multipath errors and noise, so they are thus neglected. Therefore, in this work, MP is adopted for the pseudorange multipath assessment.

2.1.4. Review on Carrier Phase Multipath Estimation

Details and characteristics of carrier-phase multipath errors can be found in [14,15,36]. Similar to the pseudorange multipath estimation, there are triple-frequency approaches for carrier-phase multipath estimation. The equation applied by Kamatham and Vemuri (2017) is similar to the one in the pseudorange multipath (i.e., Equation (1)):

$$M_{\Phi_{ijk}} = \lambda_k^2(\Phi_i - \Phi_j) + \lambda_j^2(\Phi_k - \Phi_i) + \lambda_i^2(\Phi_j - \Phi_k) \tag{6}$$

where the subscripts i, j, and k denote the three frequencies of L_i, L_j, and L_k. $M_{\Phi_{ijk}}$ denotes the ijk triple-frequency combined carrier-phase multipath error, Φ denotes the carrier-phase measurement at a frequency, and λ denotes the wavelength of a frequency. The authors of [37] used two ionosphere-free linear combinations (IF) from three frequencies to assess BDS carrier-phase errors:

$$DIF(\varphi_1, \varphi_2, \varphi_3) = IF(\varphi_1, \varphi_2) - IF(\varphi_1, \varphi_3) \tag{7}$$

This triple-carrier combination is geometry-free and ionosphere-free. The determined carrier-phase error contains the carrier-phase multipath error, measurement noise, and the linear combined carrier-phase ambiguity constant. The error determined by this approach is very "noisy" because it contains three carrier-phase measurements and three linear combinations (i.e., two iono-free combinations and one differencing). Moreover, the availability of triple-frequency is not common at CORS stations. This approach is not suitable for the work of this paper because carrier-phase multipath errors and measurement noise of individual frequencies at a CORS station cannot be estimated (i.e., the data quality information determined using the triple-carrier combination method is not suitable for single- or dual-frequency GNSS users).

Signal-to-noise ratio (SNR) and carrier-to-noise ratio (CNR) are the ratios of the signal/carrier strength to the noise level. SNR/CNR are affected by the multipath effect and atmospheric and hardware noise [15,36]. Therefore, SNR/CNR can be used to estimate/mitigate carrier-phase multipath errors [36,38]. Raw SNR/CNR data and measurement noise change with the change in satellite elevation angle. Special treatment is needed to make the raw SNR/CNR data represent the multipath-contaminated component. Special treatments include, for example, the use of elevation-dependent nominal SNR/CNR [36] and wavelet analysis [39]. Therefore, raw SNR/CNR data cannot be used to represent the data quality of carrier-phase measurements directly.

2.2. Proposed Approach for CORS Data Quality Assessment

CORS data quality assessment methods should be easy to implement at administration centers/organizations (no commercial software is needed) and ready for GNSS users with different frequencies. Pseudorange data quality information is useful for stand-alone positioning/navigation users (including mass-market users) and Differential GNSS (DGNSS) users. Carrier-phase data quality information is useful for high-precision positioning users. This section describes the proposed methods to obtain pseudorange multipath severity information, carrier-phase multipath severity information, and carrier-phase noise levels of a CORS station.

2.2.1. Pseudorange Multipath Errors

The MP approach (i.e., Equation (5)) is adopted to estimate the pseudorange multipath errors in GNSS frequencies. Two frequencies are required to calculate the pseudorange multipath error for one of the frequencies. The frequency pairs used in the case studies in this paper are shown in Table 2.

Table 2. Frequency pairing for pseudorange multipath calculation.

		GPS			**GLONASS**			**GALILEO**			**BDS**
f_1	L1	L2	L5	G1	G2	E1	E5a	E5b	E5	B1	B2
f_2	L2	L1	L1	G2	G1	E5a	E1	E1	E1	B2	B1

CORS administration centers/organizations and readers may write a simple script for Equation (5) with any computer programming language, with MATLAB, or using a spreadsheet (a RINEX reader is needed) to implement this method.

2.2.2. Carrier-Phase Multipath Errors

Obtaining the magnitude of multipath errors in carrier-phase measurements at a CORS station is non-trivial. Similar to pseudorange measurements, multipath errors in carrier-phase measurements are much smaller than the atmospheric biases, satellite orbits, and clock errors. Differencing must be used to obtain "accurate" carrier-phase residuals for multipath error analysis. For short to medium baselines, the carrier-phase residuals contain mainly multipath errors and measurement errors/random noise. With the aim of obtaining the carrier-phase multipath errors in the non-linear combined mode, the ionospheric-free combination must be avoided in the observable for residual analysis. Since the data quality assessment can be carried out in post-processing mode, the IONosphere map EXchange (IONEX) files are used to correct the ionospheric effect on GNSS measurements in our proposed approach in this paper. Regarding the tropospheric delay, the zenith tropospheric delay (ZTD) and gradient are estimated in data processing [40,41]. The double difference (DD) carrier-phase residuals are then processed by wavelets in order to remove the DD measurement noise and obtain the DD multipath errors. As a DD measurement involves four measurements at two stations and the carrier-phase multipath error is partly proportional to the PRN code correlation function [16], MPs at the two stations are used to "scale" the DD carrier-phase multipath error to form the single-differencing (SD) carrier-phase multipath error of each of the two stations at the baseline. Since the reference satellite in relative positioning is usually at high elevation angles, the multipath effect can be neglected. Therefore, the SD multipath error can be assumed as the carrier-phase multipath error of the roving satellite and station. This process is shown in Figure 2 (the upper path is highlighted with a pale blue shadow).

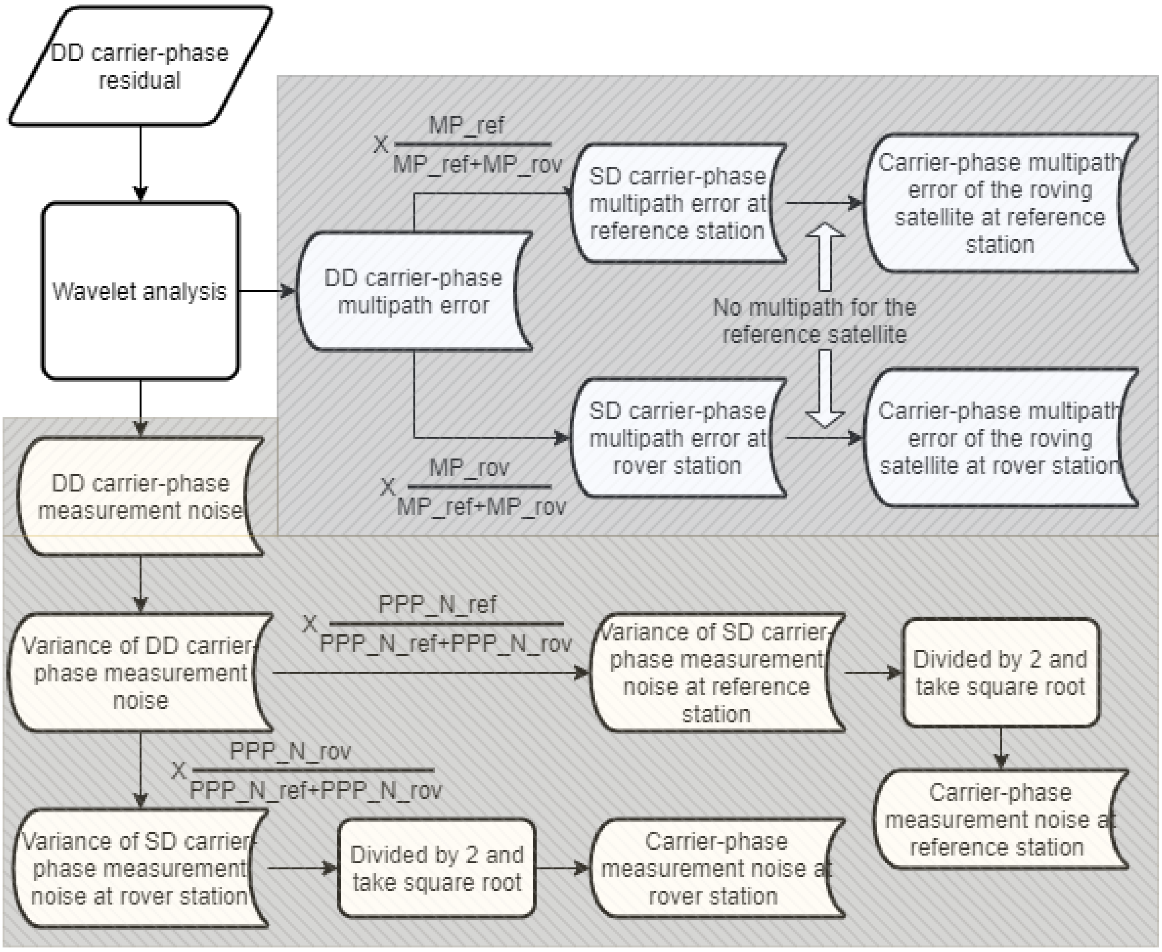

Figure 2. The process for obtaining the carrier-phase multipath error and measurement noise at an epoch. MP_ref and MP_rov denote the pseudorange multipath errors at the reference and rover stations, respectively. PPP_N_ref and PPP_N_rov denote the PPP-determined noise levels at the reference and rover CORS stations, respectively.

PPP carrier-phase residuals cannot be used to obtain carrier-phase multipath errors because pseudorange multipath errors and noise are much greater than the carrier-phase multipath errors: two orders greater. Assuming low carrier-phase multipath errors at the reference station in differencing can obtain more accurate carrier-phase multipath errors at the rover compared to using the PPP residuals. Criteria for selecting the reference station in differencing are: (1) A station with low pseudorange multipath errors (higher priority), (2) the location of the station in a group of stations (i.e., about the center of a group of stations).

CORS administration centers/organizations and readers may use the "Fixed Static" processing mode in RTKLib Demo5 b34_d3 [42,43] to output DD carrier-phase residuals, which is the input of the flowchart in Figure 2. DD carrier-phase residuals are obtained in the ".pos" output file, in MATLAB, or open-source. Since carrier-phase multipath errors at a static station show sinusoidal patterns [16], spectral analysis approaches such as Fourier transforms and wavelets can be used to separate the multipath "signal" from the noise. Wavelet analysis tools can be used to obtain the DD carrier-phase multipath errors and noise [18]. This work uses DWT and IDWT functions of the MATLAB Wavelet toolbox. The further operations in the pale blue highlighted box (i.e., for carrier-phase multipath errors) can be carried out in spreadsheets or sample programming scripts. CORS administration centers/organizations can, of course, code up the above algorithm into a piece of software with any computer programming language.

2.2.3. Carrier-Phase Measurement Noise

In the theory of errors, carrier-phase measurement noise is random noise. Carrier-phase measurement noise is usually very small; it should be within one millimeter in a carrier-phase measurement in consideration of the receiver tracking hardware. Double-difference zero-baseline method is commonly used to determine the receiver noise level [27,44]. In practice, the environments of CORS stations may introduce noise into GNSS measurements, such as radio/electrical/electronic interference-induced noise. External/environmental biases and errors (including multipath and noise) are canceled out in zero-baseline analyses. Therefore, zero-baseline methods cannot be used to quantify the CORS multipath errors and measurement noises. Low-elevation-angle satellite measurements have greater noise due to greater atmospheric noise. Therefore, we only used double-difference baseline measurements collected above a 40° satellite elevation angle in this noise analysis. An example of using the double-difference approach in noise analysis can be found in [45]. As in Section 2.2.2, CORS administration centers/organizations and readers may use RTKLib and MATLAB Wavelet toolbox to obtain the carrier-phase measurement noise. Instead of obtaining the carrier-phase multipath errors with the MATLAB DWT and IDWT functions, we obtained the filtered noise (carrier-phase measurement noise) this time. As the DD noise involves four measurements at two stations, PPP-estimated pseudorange noise at the two stations is used to "scale" the DD carrier-phase noise to form the single-differencing (SD) carrier-phase noise of each of the two stations at the baseline. This step can be carried out in spreadsheets or sample programming scripts. RTKLib's "PPP Fixed" solution (the station coordinates are known) can be used to estimate the PPP pseudorange noise; this is the method used in this work. CORS administration centers/organizations can, of course, code up the above algorithm into a piece of software with any computer programming language.

3. Case Studies

3.1. Case Study in Hong Kong

In Hong Kong, the Geodetic Survey Section of the Survey and Mapping Office (SMO) built the Hong Kong Satellite Positioning Reference Station Network (SatRef), which provides real-time network RTK and DGNSS correction data and GNSS raw data for users through 18 reference stations. The station information (receiver, antenna, and monument type) of SatRef is shown in Table 3. The authors of [46] suggested that users choose a reference station for forming a baseline within 20 km.

Table 3. Station information for the Hong Kong SatRef stations (stations are arranged by the type of monument).

Site ID	Receiver	Antenna	Type of Monument
HKKT	Leica GR50	LEIAR25.R4 LEIT	Concrete block, hilltop
HKLT	Leica GR50	LEIAR25.R4 LEIT	Concrete block, hilltop
HKMW	Trimble NetR9	LEIAR25.R4 LEIT	Concrete block, hilltop
HKNP	Leica GR50	LEIAR25.R4 LEIT	Concrete block, hilltop
HKOH	Leica GR50	LEIAR25.R4 LEIT	Concrete block, hilltop

Table 3. *Cont.*

Site ID	Receiver	Antenna	Type of Monument
HKSL	Leica GR50	LEIAR25.R4 LEIT	Concrete block, hilltop
HKSS	Leica GR50	LEIAR25.R4 LEIT	Concrete block, hilltop
HKST	Leica GR50	LEIAR25.R4 LEIT	Concrete block, hilltop
HKWS	Leica GR50	LEIAR25.R4 LEIT	Concrete block, hilltop
HKCL	Trimble NetR9	TRM59800.00 SCIT	Concrete block on building roof
HKKS	Leica GR50	TRM59800.00 SCIS	Concrete block on building roof
HKLM	Leica GR50	TRM59800.00 SCIS	Concrete block on building roof
HKPC	Leica GR50	LEIAR25.R4 LEIT	Concrete block on building roof
HKQT	Trimble NetR9	TRM59800.00 SCIT	Concrete block on building roof
HKSC	Leica GR50	LEIAR25.R4 LEIT	Concrete block on building roof
HKTK	Leica GR50	TRM59800.00 SCIS	Concrete block on building roof
KYC1	Trimble NetR9	TRM57971.00 NONE	Concrete block on building roof
T430	Leica GR50	TRM59800.00 SCIT	Concrete block on building roof

Data Description

One of the multipath characteristics is that the pattern of the multipath repeats every satellite orbital cycle. Among the four GNSS systems, Galileo satellites have the longest satellite repeat period, excluding the abnormal cases of satellites E14 and E18 [47], which have a ten-day period. Therefore, a period of 10 days was selected as the observation period per month. Moreover, six months of data are used for the data quality assessment in order to cover all possible satellite–reflector–antenna geometries (i.e., different multipath errors) at a site.

Considering the available SatRef GNSS raw data format and the support of each data format for the GNSS systems, RINEX 3.02 was chosen to obtain GPS, GLONASS, Galileo, and BDS signals. Moreover, the smallest available observation interval, 1 s, was chosen in order to better thoroughly investigate the multipath effect. The summary of the GNSS observation files is shown in Table 4.

Table 4. Observation/data file information of the GNSS data quality assessment of the Hong Kong SatRef services.

Date	Time Period per Day	File Length	Interval	Data Format
1–10 July 2020	0000–2400 (UTC)	1 h	1 s	RINEX 3.02
1–10 August 2020				
1–10 September 2020				
1–10 October 2020				
1–10 November 2020				
1–10 December 2020				

Pseudorange multipath errors, carrier-phase multipath errors, and carrier-phase measurement noise of GPS, GLONASS, Galileo, and BDS measurements of the SatRef stations at a 95% confidence level are shown in Tables A1–A3, respectively. The GPS, GLONASS, Galileo, and BDS data quality results per type of monument, receiver, and antenna are shown in Tables A4–A15.

3.2. Case Study of the Selected IGS/CORS Stations in Canada and the USA

Fourteen IGS stations were selected for this case study; they are listed in the first column of Table 5 with the station hardware information. The summary of the GNSS observation files is shown in Table 6. Pseudorange multipath errors, carrier-phase multipath errors, and carrier-phase measurement noise of GPS and GLONASS at the selected stations at a 95% confidence level are shown in Tables A17 and A18, respectively.

Table 5. Station information of the selected CRTN CORS stations.

Site ID	Receiver	Antenna Radome	Type of Monument
ALBH	SEPT POLARX5	TRM59800.00 SCIS	Concrete pier, bedrock
BAMF	SEPT POLARX5	SEPCHOKE_B3E6 SPKE	Stainless steel pedestal, bedrock
BREW	SEPT POLARX5TR	ASH701945C_M SCIT	Steel mast, sand
CHWK	SEPT POLARX5	SEPCHOKE_B3E6 SPKE	Stainless steel pedestal, crushed gravel on bedrock
DRAO	SEPT POLARX5	TWIVC6050 SCIS	Pillar/brass, bedrock
DUBO	SEPT POLARX5	AOAD/M_T NONE	Pillar/brass, bedrock
FLIN	SEPT POLARX5	NOV750.R4 NOVS	Concrete pier, bedrock
HOLB	SEPT POLARX5	SEPCHOKE_B3E6 SPKE	Concrete pier, bedrock
JPLM	SEPT POLARX5	AOAD/M_T NONE	Brass plate
NANO	SEPT POLARX5	SEPCHOKE_B3E6 SPKE	Pillar/brass, bedrock
PRDS	JAVAD TRE_3N DELTA	AOAD/M_T NONE	Brass plate
SASK	JAVAD TRE_G3TH DELTA	NOV750.R4 NOVS	Concrete pillar, gravel
UCLU	SEPT POLARX5	SEPCHOKE_B3E6 SPKE	Concrete pier, bedrock
WILL	SEPT POLARX5	SEPCHOKE_B3E6 SPKE	Pillar/brass, bedrock

Table 6. Observation/data file information of the GPS data quality assessment of the selected IGS stations in Canada/USA.

Date	Time Period Per Day	File Length	Interval	Data Format
1–10 July 2020	0000–2400 (UTC)	15 min	1 s	RINEX 2.11
1–10 August 2020				
1–10 September 2020				
1–10 October 2020				
1–10 November 2020				
1–10 December 2020				

4. Discussion

The magnitudes of multipath errors and noise shown in Tables A1–A4, A17 and A18, are not absolute. However, we know the relative error and noise levels of the CORS stations. With the relative error/noise levels of the rover/unknown station's nearby CORS stations, we can select higher-quality CORS station(s) for baseline/network-based data processing.

With the statistical data on the types of monument/receiver/antenna of the Hong Kong SatRef CORS stations in Tables A5–A15, we have made the following observations.

1. According to the statistical data shown in Tables A5–A8 about the type of monument, stations on building roofs have lower carrier-phase noise than hilltop stations. However, building-top stations have greater pseudorange and carrier-phase multipath errors (in terms of magnitude; all frequencies) than hilltop stations, except BDS. Usually, there are more reflective surfaces/materials on the roofs of buildings, so they are more likely to have a multipath effect.
2. Based on the statistical data shown in Tables A9–A12 about the type of receiver, Trimble NetR9 has lower carrier-phase noise than Leica GR50. However, Leica GR50 has a lower pseudorange and fewer carrier-phase multipath errors than Trimble NetR9. The Leica GR50 receiver may have a better multipath mitigation design in tracking loops. However, a long integration time in multipath-mitigating tracking increases the noise level [15].
3. From the statistical data shown in Tables A13–A16 about the type of antenna, Leica AR25 (LEIAR25.R4 LEIT) has slightly greater carrier-phase noise than Trimble TRM59800/TRM57971. However, Leica AR25 has a lower pseudorange and fewer carrier-phase multipath errors than Trimble TRM59800/TRM57971.00. Leica AR25 antenna may have better multipath mitigation capability.

Note that no statistics and percentage differences are given because GNSS systems have different satellite orbits and signals/frequencies; only overall performance/observations are given.

Since there are many combinations of the types of monuments/receivers/antennas at the selected IGS stations in the USA/Canada, there is not much we can draw from the results. We can only see that AOAD/M_T NONE and NOV750.R4 NOVS antennas have more significant carrier-phase multipath errors, as shown at the DUBO, FLIN, PRDS, and SASK stations in Tables A17 and A18.

Multipath and measurement noise are site environment dependent. Therefore, individual site environment inspection/analysis are outside the scope of this work. Station administrators should try to minimize the multipath effect and measurement noise if the values of the assessment metrics are large.

5. Conclusions

GNSS Continuously Operating Reference Stations (CORS) are used for determining the positions of objects in professional/engineering/scientific applications or establishing new control stations in geodetic and engineering surveying. Any errors at the CORS stations will be propagated to the rover/unknown stations, and they will also affect the network RTK methods for raw data/corrections to be applied at rovers. Currently, data quality information on carrier-phase measurements of CORS stations is not provided by station administrators, and the approach to estimating carrier-phase data quality at CORS stations is missing in the literature. Therefore, the motivation of this paper was to propose a comprehensive and practical approach to estimate the GNSS data quality at CORS stations, and the data quality information should be useful for different applications/users, such as single-frequency users. A GNSS CORS data quality assessment approach was proposed and demonstrated with CORS networks in Hong Kong and some selected IGS stations in the USA/Canada. The implementation methods (software and computer tools) of the assessment metrics have been described. Case studies of the CORS stations of the Hong Kong Satellite Positioning Reference Station Network (SatRef) and 14 IGS stations in the USA/Canada were carried out. The data quality metrics of the CORS stations estimated by the proposed approach are the carrier-phase measurement noise, pseudorange, and carrier-phase multipath errors; no validation of the proposed approach is possible because the "true" errors and noise are never known. Note that the magnitudes of multipath errors and noise are not absolute. However, the relative error and noise levels of the CORS stations can serve as the purpose of quality checks among CORS stations. In the case studies, some stations have significantly greater carrier-phase measurement noise than other stations in the same CORS network. This may indicate that there are problems with the instruments and/or the environments of the stations. In such cases, the station administrator should check the hardware and software at the station(s); for example, the data quality of SatRef's HKLT station is poor. The estimated pseudorange and carrier-phase multipath errors can be used as indicators of the multipath severity of CORS stations for DGNSS and RTK services, respectively. DGNSS and RTK service providers/users can select low multipath-severity CORS stations as the reference station(s) in single-station-based or network-based DGNSS and RTK approaches. All CORS stations ought to provide data quality information to users.

Author Contributions: Conceptualization, L.L. and K.-W.T.; methodology, K.-W.T. and L.L.; software, K.-W.T.; validation, K.-W.T.; formal analysis, K.-W.T. and L.L.; investigation, K.-W.T. and L.L.; resources, L.L.; data curation, K.-W.T. and L.L.; writing—original draft preparation, K.-W.T. and L.L.; writing—review and editing, L.L.; visualization, K.-W.T. and L.L.; supervision, L.L.; project administration, L.L.; funding acquisition, L.L. All authors have read and agreed to the published version of the manuscript.

Funding: This research was funded by the Startup funds of the Hong Kong Polytechnic University, grant number 1-BD6G.

Data Availability Statement: All SatRef data used in this article are available at: https://www.geodetic.gov.hk/en/rinex/ftp_RINEX.htm (accessed on 20 February 2023). All IGS data used in this article are available at: https://cddis.nasa.gov/archive/gnss/data/highrate (accessed on 20 February 2023).

Conflicts of Interest: The authors declare no conflict of interest.

Appendix A

Table A1. Carrier-phase measurement noise, pseudorange, and carrier-phase multipath errors of the Hong Kong SatRef GPS three-frequency measurements at a 95% confidence level.

Station ID	Carrier-Phase Measurement Noise (mm)			Carrier-Phase Multipath Error (mm)			Pseudorange Multipath Error (m)		
	L1	L2	L5	L1	L2	L5	L1	L2	L5
HKCL	0.6	0.7	0.6	13.3	15.3	18.6	0.404	0.408	0.427
HKKS	0.4	0.5	0.3	6	8.3	7.1	0.196	0.251	0.464
HKKT	0.5	0.5	0.3	7	8.1	8.4	0.283	0.26	0.715
HKLM	0.5	0.6	0.4	8.9	14	17.6	0.267	0.323	0.765
HKLT	3.3	3.9	4.7	6.5	7.9	8.4	0.249	0.213	0.583
HKMW	0.7	0.8	0.6	11.4	14.3	14.6	0.415	0.397	0.471
HKNP	0.5	0.5	0.5	11.1	12.7	13	0.278	0.257	0.621
HKOH	0.5	0.5	0.3	10.1	10	8.7	0.255	0.22	0.225
HKPC	0.5	0.5	0.3	11.3	12.7	13.3	0.292	0.27	0.296
HKQT	0.5	0.6	0.4	7.8	7.9	7.4	0.492	0.558	0.381
HKSC	0.5	0.5	0.3	6.5	6.9	8.1	0.238	0.213	0.237
HKSL	0.5	0.6	0.3	11	13.2	11.5	0.259	0.25	0.279
HKSS	0.5	0.5	0.3	6.3	7.2	6.8	0.232	0.21	0.616
HKST	0.5	0.5	0.3	7.5	8	8.3	0.276	0.255	0.276
HKTK	0.5	0.5	0.4	8.4	9.4	9.4	0.3	0.29	0.218
HKWS	0.5	0.5	0.3	8.1	9.8	10.1	0.3	0.244	0.288
KYC1	0.6	0.7	0.5	11.9	12.9	15.8	0.327	0.293	0.334
T430	0.5	0.5	0.3	8.4	14.5	14	0.273	0.289	0.304

Table A2. Carrier-phase measurement noise, pseudorange, and carrier-phase multipath errors of the Hong Kong SatRef GLONASS dual-frequency measurements at a 95% confidence level.

Station ID	Carrier-Phase Measurement Noise (mm)		Carrier-Phase Multipath Error (mm)		Pseudorange Multipath Error (m)	
	L1	L2	L1	L2	L1	L2
HKCL	0.6	1.8	26.1	29	0.551	0.288
HKKS	0.4	0.4	5.3	6.5	0.168	0.204
HKKT	0.5	0.5	7.6	9.3	0.313	0.27
HKLM	0.5	0.6	7.7	9.4	0.209	0.234
HKLT	3.2	3.5	5.6	6.7	0.257	0.217
HKMW	0.7	0.8	30.7	23.7	0.65	0.372
HKNP	0.5	0.5	12.5	14	0.279	0.242
HKOH	0.6	0.6	6.7	7.2	0.255	0.223
HKPC	0.5	0.5	10.7	9.5	0.32	0.281
HKQT	0.8	0.8	24.9	18.7	0.534	0.25
HKSC	0.5	0.5	6.2	6.7	0.285	0.248
HKSL	0.5	0.5	9.5	11.7	0.264	0.268
HKSS	0.4	0.5	8.9	9	0.229	0.203
HKST	0.5	0.5	6.8	7.8	0.301	0.266
HKTK	1.2	1.2	25.9	23.9	0.425	0.209
HKWS	0.4	0.5	7.7	9	0.323	0.262
KYC1	1.2	1	25.4	26.2	0.533	0.512
T430	2	2.5	5.4	6.2	0.273	0.29

Table A3. Carrier-phase measurement noise, pseudorange, and carrier-phase multipath errors of the Hong Kong SatRef Galileo three-frequency measurements at a 95% confidence level.

Station ID	Measurement Noise (mm)			Carrier-Phase Multipath Error (mm)			Pseudorange Multipath Error (m)			
	E1	E5a	E5b	E1	E5a	E5b	E1	E5a	E5b	E5
HKCL	0.7	0.7	0.7	16.4	16.6	18.2	0.233	0.3	0.339	1.025
HKKS	0.3	0.3	0.3	11.3	12.6	11.9	0.355	0.414	0.414	0.39
HKKT	0.4	0.4	0.3	11	10.7	10.6	0.353	0.372	0.363	0.286
HKLM	1	1	1	27.4	22.6	23.3	0.32	0.395	0.385	0.349
HKLT	3.5	4	3.8	7.5	8.5	8	0.338	0.34	0.334	0.268
HKMW	0.6	0.6	0.5	20.5	20.4	21.5	0.334	0.451	0.505	1.254
HKNP	0.4	0.4	0.4	16.1	17.4	17.9	0.279	0.304	0.323	0.203
HKOH	0.4	0.4	0.4	12.6	14	14	0.265	0.266	0.256	0.182
HKPC	0.4	0.4	0.3	14.7	15.5	17.1	0.286	0.335	0.355	0.215
HKQT	0.5	0.5	0.4	14.8	14.7	13.8	0.189	0.231	0.246	1.178
HKSC	0.4	0.4	0.3	14.1	14.1	14.3	0.684	0.684	0.679	0.685
HKSL	0.4	0.4	0.4	17.6	19.5	16.4	0.329	0.365	0.494	0.293
HKSS	0.4	0.3	0.3	11	10.6	10.5	0.233	0.249	0.248	0.15
HKST	0.4	0.4	0.3	12.1	14.3	12.9	0.26	0.298	0.3	0.187
HKTK	0.4	0.4	0.4	19.5	19.1	18.9	0.222	0.278	0.291	0.243
HKWS	0.4	0.3	0.3	15.5	14.4	16.9	0.271	0.291	0.295	0.15
KYC1										
T430	0.4	0.3	0.3	12.7	13.8	12.1	0.607	0.72	0.728	0.703

Table A4. Carrier-phase measurement noise, pseudorange, and carrier-phase multipath errors of the Hong Kong SatRef BDS B1 and B2 measurements at a 95% confidence level.

Station ID	Carrier-Phase Measurement Noise (mm)						Carrier-Phase Multipath Error (mm)						Pseudorange Multipath Error (m)					
	MEO		GEO		IGSO		MEO		GEO		IGSO		MEO		GEO		IGSO	
	B1	B2	B1	B2	B1	B2	B1	B2	B1	B2	B1	B2	B1	B2	B1	B2	B1	B2
HKCL	0.3	0.3	0.7	0.8	0.4	0.5	2.9	3.7	6.4	7.1	4	5.3	0.448	0.288	0.312	0.16	0.311	0.211
HKKS	0.2	0.2	0.5	0.5	0.3	0.3	1.8	2.7	3.4	5.6	2.7	4.4	0.328	0.279	0.067	0.071	0.192	0.183
HKKT	0.2	0.2	0.6	0.5	0.4	0.3	2.5	3.2	5.4	6.9	3.4	4.9	0.409	0.303	0.237	0.304	0.32	0.233
HKLM	0.2	0.2	0.5	0.5	0.3	0.3	3.1	4.6	4.4	5.9	3.2	4.6	0.355	0.278	0.079	0.086	0.244	0.241
HKLT	1	1.4	2.2	2.8	1.7	2.1	2.1	2.7	4.2	5.8	3.1	4.2	0.386	0.281	0.224	0.159	0.276	0.199
HKMW	0.3	0.3	0.7	0.8	0.5	0.5	3.7	4.6	7	8.3	4.1	5.3	0.531	0.34	0.362	0.249	0.389	0.271
HKNP	0.2	0.2	0.6	0.6	0.4	0.4	2.4	3.4	5.6	7.4	3.8	5.3	0.393	0.283	0.191	0.188	0.335	0.298
HKOH	0.2	0.2	0.5	0.5	0.4	0.3	3.8	4.8	4.5	5.6	3.1	4.1	0.392	0.263	0.263	0.217	0.303	0.213
HKPC	0.2	0.2	0.5	0.5	0.4	0.3	2.6	3.4	5.7	7.1	3.2	4.7	0.402	0.309	0.334	0.218	0.321	0.264
HKQT	0.2	0.3	0.6	0.7	0.4	0.4	3.3	3.3	4.5	5.1	2.6	3.5	0.428	0.273	0.291	0.16	0.221	0.178
HKSC	0.2	0.2	0.5	0.5	0.4	0.3	2.2	2.8	4.5	5.1	2.9	3.9	0.357	0.249	0.288	0.245	0.342	0.309
HKSL	0.2	0.2	0.6	0.6	0.4	0.4	3.1	3.7	5.2	7.1	3.6	5.2	0.368	0.273	0.259	0.175	0.306	0.283
HKSS	0.2	0.2	0.5	0.5	0.4	0.3	2.2	2.7	4.8	6.3	3.1	4.2	0.368	0.271	0.302	0.233	0.284	0.21
HKST	0.2	0.2	0.5	0.5	0.4	0.3	2.6	3.6	5.2	6.6	3.3	4.4	0.398	0.291	0.252	0.206	0.321	0.233
HKTK	0.2	0.2	0.6	0.6	0.4	0.4	3	3.5	5.2	6.3	2.8	3.4	0.394	0.247	0.291	0.13	0.276	0.206
HKWS	0.2	0.2	0.6	0.5	0.4	0.4	3.1	3.7	5.5	6.7	3.8	5.3	0.413	0.311	0.271	0.284	0.321	0.229
KYC1																		
T430	0.2	0.2	0.5	0.5	0.3	0.3	2.4	3.1	4.4	5.6	2.9	3.7	0.369	0.311	0.05	0.052	0.268	0.27

Table A5. GPS data quality of SatRef stations per type of monument at a 95% confidence level.

Type of Monument	Number of Stations	Carrier-Phase Measurement Noise (mm)			Carrier-Phase Multipath Error (mm)			Pseudorange Multipath Error (m)		
		L1	L2	L5	L1	L2	L5	L1	L2	L5
Hilltop	9	1.2	1.4	1.6	9	10.4	10.3	0.287	0.262	0.486
Rooftop	9	0.5	0.6	0.4	9.4	11.7	13.1	0.321	0.336	0.411

Table A6. GLONASS data quality of SatRef stations per type of monument at a 95% confidence level.

Type of Monument	Number of Stations	Carrier-Phase Measurement Noise (mm)		Carrier-Phase Multipath Error (mm)		Pseudorange Multipath Error (m)	
		R1	R2	R1	R2	R1	R2
Hilltop	9	1.2	1.3	12.9	12	0.341	0.262
Rooftop	9	1	1.2	17.9	17.5	0.392	0.293

Table A7. Galileo data quality of SatRef stations per type of monument at a 95% confidence level.

Type of Monument	Number of Stations	Carrier-Phase Measurement Noise (mm)			Carrier-Phase Multipath Error (mm)			Pseudorange Multipath Error (m)			
		E1	E5a	E5b	E1	E5a	E5b	E1	E5a	E5b	E5
Hilltop	9	1.2	1.4	1.3	14.3	14.9	14.9	0.299	0.332	0.357	0.467
Rooftop	9	0.5	0.5	0.5	17	16.4	16.6	0.401	0.454	0.46	0.688

Table A8. BDS data quality of SatRef stations per type of monument at a 95% confidence level.

Type of Monument	Number of Stations	Carrier-Phase Measurement Noise (mm)						Carrier-Phase Multipath Error (mm)						Pseudorange Multipath Error (m)					
		MEO		GEO		IGSO		MEO		GEO		IGSO		MEO		GEO		IGSO	
		B1	B2	B1	B2	B1	B2	B1	B2	B1	B2	B1	B2	B1	B2	B1	B2	B1	B2
Hilltop	9	0.4	0.5	0.9	1.1	0.7	0.8	2.9	3.7	5.3	6.8	3.5	4.8	0.409	0.292	0.266	0.228	0.319	0.243
Rooftop	9	0.2	0.2	0.6	0.6	9.6	0.4	2.7	3.4	4.9	6	3.1	4.2	0.387	0.28	0.243	0.154	0.276	0.237

Table A9. GPS data quality of SatRef stations per type of receiver at a 95% confidence level.

Type of Receiver	Number of Stations	Carrier-Phase Measurement Noise (mm)			Carrier-Phase Multipath Error (mm)			Pseudorange Multipath Error (m)		
		L1	L2	L5	L1	L2	L5	L1	L2	L5
Leica GR50	14	1.0	1.1	1.3	8.6	10.5	10.8	0.266	0.255	0.462
Trimble NetR9	4	0.6	0.7	0.4	11.3	12.9	14.7	0.414	0.425	0.406

Table A10. GLONASS data quality of SatRef stations per type of receiver at a 95% confidence level.

Type of Receiver	Number of Stations	Carrier-Phase Measurement Noise (mm)		Carrier-Phase Multipath Error (mm)		Pseudorange Multipath Error (m)	
		R1	R2	R1	R2	R1	R2
Leica GR50	14	1.1	1.3	10.4	10.7	0.285	0.246
Trimble NetR9	4	0.9	1.2	26.9	24.7	0.569	0.369

Table A11. Galileo data quality of SatRef stations per type of receiver at a 95% confidence level.

Type of Receiver	Number of Stations	Carrier-Phase Measurement Noise (mm)			Carrier-Phase Multipath Error (mm)			Pseudorange Multipath Error (m)			
		E1	E5a	E5b	E1	E5a	E5b	E1	E5a	E5b	E5
Leica GR50	14	1	1.1	1.2	15.2	15.1	15.2	0.367	0.404	0.415	0.352
Trimble NetR9	4	0.6	0.5	0.6	17.4	18.1	17.4	0.259	0.34	0.378	1.156

Table A12. BDS data quality of SatRef stations per type of receiver at a 95% confidence level.

Type of Receiver	Number of Stations	Carrier-Phase Measurement Noise (mm)						Carrier-Phase Multipath Error (mm)						Pseudorange Multipath Error (m)					
		MEO		GEO		IGSO		MEO		GEO		IGSO		MEO		GEO		IGSO	
		B1	B2	B1	B2	B1	B2	B1	B2	B1	B2	B1	B2	B1	B2	B1	B2	B1	B2
Leica GR50	14	0.3	0.4	0.8	0.9	7.3	0.7	2.7	3.5	4.9	6.3	3.2	4.5	0.382	0.283	0.239	0.198	0.296	0.244
Trimble NetR9	4	0.3	0.3	0.7	0.8	0.4	0.5	3.3	3.9	6.1	7	3.6	4.8	0.471	0.302	0.323	0.194	0.315	0.223

Table A13. GPS data quality of SatRef stations per type of antenna at a 95% confidence level.

Type of Antenna	Number of Stations	Carrier-Phase Measurement Noise (mm)			Carrier-Phase Multipath Error (mm)			Pseudorange Multipath Error (m)		
		L1	L2	L5	L1	L2	L5	L1	L2	L5
LEIAR25.R4 LEIT	11	1.1	1.3	1.5	9	10.4	10.4	0.284	0.258	0.454
TRM59800.00 SCIT	3	0.5	0.6	0.4	10.1	13	14.1	0.4	0.433	0.374
TRM59800.00 SCIS	3	0.5	0.5	0.4	7.9	10.9	12.2	0.258	0.29	0.532
TRM57971.00 NONE	1	0.7	0.7	0.5	11.9	12.9	15.8	0.327	0.293	0.334

Table A14. GLONASS data quality of SatRef stations per type of antenna at a 95% confidence level.

Type of Antenna	Number of Stations	Carrier-Phase Measurement Noise (mm)		Carrier-Phase Multipath Error (mm)		Pseudorange Multipath Error (m)	
		R1	R2	R1	R2	R1	R2
LEIAR25.R4 LEIT	11	1.1	1.2	12.3	11.4	0.334	0.263
TRM59800.00 SCIT	3	1.3	1.8	21.1	20.2	0.47	0.277
TRM59800.00 SCIS	3	0.8	0.8	15.9	15.3	0.29	0.216
TRM57971.00 NONE	1	1.2	1	25.4	26.2	0.533	0.512

Table A15. Galileo data quality of SatRef stations per type of antenna at a 95% confidence level.

Type of Antenna	Number of Stations	Carrier-Phase Measurement Noise (mm)			Carrier-Phase Multipath Error (mm)			Pseudorange Multipath Error (m)			
		E1	E5a	E5b	E1	E5a	E5b	E1	E5a	E5b	E5
LEIAR25.R4 LEIT	11	1.1	1.2	1.3	14.3	15	14.9	0.351	0.378	0.397	0.475
TRM59800.00 SCIT	3	0.5	0.5	0.5	14.7	14.9	15.1	0.391	0.47	0.485	0.989
TRM59800.00 SCIS	3	0.6	0.6	0.6	20.5	18.6	18.6	0.304	0.367	0.367	0.333

Table A16. BDS data quality of SatRef stations per type of antenna at a 95% confidence level.

Type of Antenna	Number of Stations	Carrier-Phase Measurement Noise (mm)						Carrier-Phase Multipath Error (mm)						Pseudorange Multipath Error (m)					
		MEO		GEO		IGSO		MEO		GEO		IGSO		MEO		GEO		IGSO	
		B1	B2	B1	B2	B1	B2	B1	B2	B1	B2	B1	B2	B1	B2	B1	B2	B1	B2
LEIAR25.R4 LEIT	11	0.4	0.5	0.9	1	0.6	0.7	2.8	3.6	5.3	6.7	3.4	4.7	0.404	0.289	0.275	0.229	0.321	0.252
TRM59800.00 SCIT	3	0.2	0.2	0.6	0.7	15.7	0.4	2.9	3.4	5.2	6	3.2	4.2	0.417	0.291	0.248	0.134	0.269	0.223
TRM59800.00 SCIS	3	0.2	0.2	0.5	0.5	0.3	0.3	2.7	3.7	4.4	6	2.9	4.1	0.36	0.268	0.178	0.099	0.24	0.211

Appendix B

Table A17. Carrier-phase measurement noise, pseudorange, and carrier-phase multipath errors of GPS dual-frequency measurements of the selected IGS stations at a 95% confidence level.

Station ID	Carrier-Phase Measurement Noise (mm)		Carrier-Phase Multipath Error (mm)		Pseudorange Multipath Error (m)	
	L1	L2	L1	L2	L1	L2
ALBH	0.5	0.6	12.4	15.1	0.318	0.28
BAMF	0.3	0.4	15.9	17.6	0.821	1.005
BREW	0.8	1.1	16.7	22.1	0.437	0.446
CHWK	1.1	5.1	24.5	63.7	0.596	0.544
DRAO	1.3	1.2	18.2	22.6	0.358	0.279
DUBO	0.7	13.2	16.1	117.6	0.453	0.363
FLIN	1.5	11.4	27.7	83.6	0.498	0.360
HOLB	0.7	1.0	11.9	13.0	0.366	0.428
JPLM	1.6	1.3	21.6	17.8	0.271	0.312
NANO	1.5	1.4	13	12.7	0.604	0.712
PRDS	0.9	37.3	18.1	181.2	0.310	0.354
SASK	2.2	3.0	25.0	25.0	0.274	0.313
UCLU	0.2	0.3	10.6	11.9	0.372	0.427
WILL	1.3	14.6	19.6	38.5	0.469	0.396

Table A18. Carrier-phase measurement noise, pseudorange, and carrier-phase multipath errors of GLONASS dual-frequency measurements of the selected IGS stations at a 95% confidence level.

Station ID	Carrier-Phase Measurement Noise (mm)		Carrier-Phase Multipath Error (mm)		Pseudorange Multipath Error (m)	
	L1	L2	L1	L2	L1	L2
ALBH	0.5	0.6	20.7	29.8	0.438	0.379
BAMF	0.4	1.0	12.3	15.8	1.352	1.436
BREW	0.5	0.7	14.6	17.8	0.886	1.026
CHWK	0.7	1.3	22.3	28.9	0.828	0.649
DRAO	0.3	0.4	12.1	20.6	0.432	0.399
DUBO	0.6	87.1	16.4	262.5	0.644	0.475
FLIN	0.6	0.6	18.0	21.4	0.541	0.402
HOLB	0.5	0.8	13.5	16.5	0.353	0.377
JPLM	1.3	2.9	16.6	19.0	0.996	1.136
NANO	0.5	0.7	10.0	14.5	1.090	1.242
PRDS	0.5	0.7	8.6	15.1	0.336	0.351
SASK	1.5	1.4	28.5	26.9	0.269	0.342
UCLU	0.4	1.2	8.5	12.0	1.160	1.382
WILL	0.7	1.0	18.7	24.6	0.651	0.586

References

1. Goad, C.C.; Remondi, B.W. Initial relative positioning results using the global positioning system. *Bull. Geod.* **1984**, *58*, 193–210. [CrossRef]
2. Remondi, B.W. Using the Global Positioning System (GPS) Phase Observable for Relative Geodesy: Modeling, Processing, and Results. Ph.D. Dissertation, Center for Space Research, The University of Texas at Austin, Austin, TX, USA, 1984; 360p.
3. Remondi, B.W. Global positioning system carrier phase: Description and use. *Bull. Geod.* **1985**, *59*, 361–377. [CrossRef]
4. Lu, G.; Lachapelle, G.; Cannon, M.E.; Kielland, P. Attitude Determination in a Survey Launch Using Multi-Antenna GPS Technology. In Proceedings of the National Technical Meeting of the Institute of Navigation: Evolution through Integration of Current and Emerging Systems, San Francisco, CA, USA, 20–22 January 1993; pp. 251–259.
5. Lau, L.; Cross, P.; Steen, M. Flight Tests of Error-Bounded Heading and Pitch Determination with Two GPS Receivers. *IEEE Trans. Aerosp. Electron. Syst.* **2012**, *48*, 388–404. [CrossRef]
6. Bossler, J.D.; Goad, C.C.; Bender, P.L. Using the Global Positioning System (GPS) for geodetic positioning. *Bull. Geod.* **1980**, *54*, 553–563. [CrossRef]
7. Soler, T.; Alvarez-Garcia, G.; Hernandez-Navarro, A.; Foote, R.H. GPS high accuracy geodetic networks in Mexico. *J. Surv. Eng.* **1996**, *122*, 80–94. [CrossRef]
8. Blewitt, G. Carrier Phase Ambiguity Resolution for the Global Positioning System Applied to Geodetic Baselines up to 2000 Km. *J. Geophys. Res.-Solid Earth Planets* **1989**, *94*, 10187–10203. [CrossRef]
9. Dong, D.N.; Bock, Y. Global Positioning System Network Analysis with Phase Ambiguity Resolution Applied to Crustal Deformation Studies in California. *J. Geophys. Res.-Solid Earth Planets* **1989**, *94*, 3949–3966. [CrossRef]
10. Ashkenazi, V.; Delafuente, C.; Moore, T. GPS at Nottingham-University. *J. Surv. Eng.-ASCE* **1988**, *114*, 146–155. [CrossRef]
11. Brown, N.; Keenan, R.; Richter, B.; Troyer, L. Advances in Ambiguity Resolution for RTK Applications Using the New RTCM V3.0 Master-Auxiliary Messages . In Proceedings of the 18th International Technical Meeting of the Satellite Division of The Institute of Navigation (ION GNSS 2005), Long Beach, CA, USA, 13–16 September 2005; pp. 73–80.
12. Vollath, U.; Landau, H.; Chen, X.; Doucet, K.; Pagels, C. Network RTK Versus Single Base RTK—Understanding the Error Characteristics. In Proceedings of the 15th International Technical Meeting of the Satellite Division of The Institute of Navigation (ION GPS 2002), Portland, OR, USA, 24–27 September 2002; pp. 2774–2781.
13. IGS Current IGS Site Guidelines. International GNSS Service (IGS). 2015. Available online: https://kb.igs.org/hc/en-us/articles/202011433-Current-IGS-Site-Guidelines (accessed on 13 February 2023).
14. Lau, L.; Cross, P. Investigations into phase multipath mitigation techniques for high precision positioning in difficult environments. *J. Navig.* **2007**, *60*, 457–482. [CrossRef]
15. Lau, L. GNSS Multipath Errors and Mitigation Techniques. In *GPS and GNSS Technology in Geosciences*; Elsevier: Amsterdam, The Netherlands, 2021; pp. 77–98.
16. Lau, L.; Cross, P. Development and testing of a new ray-tracing approach to GNSS carrier-phase multipath modelling. *J. Geod.* **2007**, *81*, 713–732. [CrossRef]
17. Leick, A. *GPS Satellite Surveying*, 2nd ed.; Wiley-Interscience: New York, NY, USA, 1994; ISBN 0-471-30626-6.

18. Lau, L. Wavelet packets based denoising method for measurement domain repeat-time multipath filtering in GPS static high-precision positioning. *GPS Solut.* **2017**, *21*, 461–474. [CrossRef]
19. Su, M.K.; Zheng, J.S.; Yang, Y.X.; Wu, Q. A new multipath mitigation method based on adaptive thresholding wavelet denoising and double reference shift strategy. *GPS Solut.* **2018**, *22*, 40. [CrossRef]
20. Fuhrmann, T.; Luo, X.G.; Knopfler, A.; Mayer, M. Generating statistically robust multipath stacking maps using congruent cells. *GPS Solut.* **2015**, *19*, 83–92. [CrossRef]
21. Dong, D.; Wang, M.; Chen, W.; Zeng, Z.; Song, L.; Zhang, Q.; Cai, M.; Cheng, Y.; Lv, J. Mitigation of multipath effect in GNSS short baseline positioning by the multipath hemispherical map. *J. Geod.* **2016**, *90*, 255–262. [CrossRef]
22. Estey, L.H.; Meertens, C.M. TEQC: The Multi-Purpose Toolkit for GPS/GLONASS Data. *GPS Solut.* **1999**, *3*, 42–49. [CrossRef]
23. Ogaja, C.; Hedfors, J. TEQC multipath metrics in MATLAB. *GPS Solut.* **2007**, *11*, 215–222. [CrossRef]
24. Xiao, Y.; Yao, M.H.; Tang, S.H.; Liu, H.F.; Xing, P.W.; Zhang, Y. Data quality check and visual analysis of CORS station based on ANUBIS software. *Int. Arch. Photogramm. Remote Sens. Spatial Inf. Sci.* **2020**, *42*, 1295–1300. [CrossRef]
25. Vaclavovic, P.; Dousa, J. G-Nut/Anubis: Open-Source Tool for Multi-GNSS Data Monitoring with a Multipath Detection for New Signals, Frequencies and Constellations. In *IAG 150 Years*; Rizos, C., Willis, P., Eds.; Springer International Publishing (International Association of Geodesy Symposia): Cham, Switzerland, 2016; pp. 775–782.
26. Nischan, T. GFZRNX—RINEX GNSS Data Conversion and Manipulation Toolbox. GFZ Data Services. 2016. Available online: https://doi.org/10.5880/GFZ.1.1.2016.002 (accessed on 13 February 2023).
27. Quan, Y.M.; Lau, L.; Roberts, G.W.; Meng, X.L. Measurement Signal Quality Assessment on All Available and New Signals of Multi-GNSS (GPS, GLONASS, Galileo, BDS, and QZSS) with Real Data. *J. Navig.* **2016**, *69*, 313–334. [CrossRef]
28. Cai, C.S.; He, C.; Santerre, R.; Pan, L.; Cui, X.Q.; Zhu, J.J. A comparative analysis of measurement noise and multipath for four constellations: GPS, BeiDou, GLONASS and Galileo. *Surv. Rev.* **2016**, *48*, 287–295. [CrossRef]
29. Park, K.; Kim, K.; Lim, H.; Park, P. Evaluation of data quality of permanent GPS stations in South Korea. *J. Astron. Space Sci.* **2002**, *19*, 367–376. [CrossRef]
30. Hilla, S.; Cline, M. Evaluating pseudorange multipath effects at stations in the National CORS Network. *GPS Solut.* **2004**, *7*, 253–267. [CrossRef]
31. Park, K.D.; Nerem, R.S.; Schenewerk, M.S.; Davis, J.L. Site-specific multipath characteristics of global IGS and CORS GPS sites. *J. Geod.* **2004**, *77*, 799–803. [CrossRef]
32. Kamatham, Y.; Vemuri, S.S. Analysis and Estimation of Multipath Interference using Dual and Triple Frequency GNSS Signals. In Proceedings of the 2017 IEEE Applied Electromagnetics Conference (AEMC), Aurangabad, India, 19–22 December 2017.
33. Braasch, M.S. Multipath Effects. In *Global Positioning System: Theory and Applications*; American Institute of Aeronautics and Astronautics: Washington, DC, USA, 1996; Volume I, pp. 547–568.
34. Zhdanov, A.; Veitsel, V.; Zhodzishsky, M.; Ashjaee, J. Multipath Error Reduction in Signal Processing. In Proceedings of the 12th International Technical Meeting of the Satellite Division of The Institute of Navigation (ION GPS 1999), Nashville, TN, USA, 14–17 September 1999; pp. 1217–1224.
35. Cai, C.S.; Gao, Y.; Pan, L.; Dai, W.J. An analysis on combined GPS/COMPASS data quality and its effect on single point positioning accuracy under different observing conditions. *Adv. Space Res.* **2014**, *54*, 818–829. [CrossRef]
36. Lau, L.; Cross, P. A New Signal-to-Noise-Ratio Based Stochastic Model for GNSS High-Precision Carrier Phase Data Processing Algorithms in the Presence of Multipath Errors. In Proceedings of the 19th International Technical Meeting of the Satellite Division of the Institute of Navigation (ION GNSS 2006), Fort Worth, TX, USA, 26–29 September 2006; pp. 276–285.
37. Montenbruck, O.; Hauschild, A.; Steigenberger, P.; Hugentobler, U.; Teunissen, P.; Nakamura, S. Initial assessment of the COMPASS/BeiDou-2 regional navigation satellite system. *GPS Solut.* **2013**, *17*, 211–222. [CrossRef]
38. Comp, C.J.; Axelrad, P. Adaptive SNR-based carrier phase multipath mitigation technique. *IEEE Trans. Aerosp. Electron. Syst.* **1998**, *34*, 264–276. [CrossRef]
39. Bilich, A.; Larson, K.M.; Axelrad, P. Modeling GPS phase multipath with SNR: Case study from the Salar de Uyuni, Boliva. *J. Geophys. Res.-Solid Earth* **2008**, *113*, B04401. [CrossRef]
40. Bar-Sever, Y.E.; Kroger, P.M.; Borjesson, J.A. Estimating horizontal gradients of tropospheric path delay with a single GPS receiver. *J. Geophys. Res.-Solid Earth* **1998**, *103*, 5019–5035. [CrossRef]
41. Miyazaki, S.; Iwabuchi, T.; Heki, K.; Naito, I. An impact of estimating tropospheric delay gradients on precise positioning in the summer using the Japanese nationwide GPS array. *J. Geophys. Res.-Solid Earth* **2003**, *108*, 2335. [CrossRef]
42. Takasu, T.; Yasuda, A. Development of the low-cost RTK-GPS receiver with an open source program package RTKLIB. In Proceedings of the International Symposium on GPS/GNSS, Jeju, Republic of Korea, 4–6 November 2009.
43. Everett, T. RTKLIB (Demo5 b34_d3). 2021. Available online: http://rtkexplorer.com/downloads/rtklib-code/ (accessed on 13 February 2023).
44. de Bakker, P.F.; van der Marel, H.; Tiberius, C.C.J.M. Geometry-free undifferenced, single and double differenced analysis of single frequency GPS, EGNOS and GIOVE-A/B measurements. *GPS Solut.* **2009**, *13*, 305–314. [CrossRef]
45. Amiri-Simkooei, A.R.; Tiberius, C.C.J.M. Assessing receiver noise using GPS short baseline time series. *GPS Solut.* **2007**, *11*, 21–35. [CrossRef]

46. Lands Department Specifications and Practice Guide for Establishing GPS Control Stations for Land Boundary Surveys. 2004. Available online: https://www.landsd.gov.hk/mapping/en/leg/cop/cop_v4.pdf (accessed on 13 February 2023).
47. Robustelli, U.; Benassai, G.; Pugliano, G. Signal in Space Error and Ephemeris Validity Time Evaluation of Milena and Doresa Galileo Satellites. *Sensors* **2019**, *19*, 1786. [CrossRef] [PubMed]